Eur. J. Mineral.
2013, **25**, 1017–1030
Published online December 2013

Tubulite, ~$Ag_2Pb_{22}Sb_{20}S_{53}$, a new Pb–Ag–Sb sulfosalt from Le Rivet quarry, Peyrebrune ore field (Tarn, France) and Biò, Borgofranco mines, Borgofranco d'Ivrea (Piedmont, Italy)

YVES MOËLO[1,*], ROBERT PECORINI[2], MARCO E. CIRIOTTI[3], NICOLAS MEISSER[4], MARIA TERESA CALDES[1], PAOLO ORLANDI[5], PIERRE-EMMANUEL PETIT[1], BRUNO MARTINI[6] and ADRIO SALVETTI[7]

[1] Institut des Matériaux Jean Rouxel, UMR 6502, CNRS, Université de Nantes, 2, rue de la Houssinière, F-44322 Nantes Cedex 3, France
*Corresponding author, e-mail: Yves.Moelo@cnrs-imn.fr
[2] Association Française de Microminéralogie, 9, allée des Chênes Verts, F-13620 Carry le Rouet, France
[3] Associazione Micromineralogica Italiana - via San Pietro, 55, I-10073 Devesi-Cirié, Italy
[4] Musée de géologie & Institut des sciences de la Terre, Université de Lausanne, CH-1015 Lausanne, Switzerland
[5] Dipartimento di Scienze della Terra, Università di Pisa, via S. Maria 53, I-56126 Pisa, Italy
[6] Associazione Micromineralogica Italiana - via Roma, 26, I-13812 Campiglia Cervo, Italy
[7] Associazione Micromineralogica Italiana - strada Regione Croce, 30–I-13900 Chiavazza, Italy

Abstract: Tubulite, ~ $Ag_2Pb_{22}Sb_{20}S_{53}$, is a new Pb–Ag–Sb sulfosalt discovered at Le Rivet quarry, Peyrebrune ore field (Tarn, France) and Biò, Borgofranco mines, Borgofranco d'Ivrea (Piedmont, Italy). As indicated by the name, it forms very thin perfect micro-tubes, 100 to 600 μm in length, 40 to 100 μm in diameter, and only 1 to 2 μm in thickness; a hair-like variety is also present at Biò. At Le Rivet, it is associated with galena, pyrite, pyrrhotite, arsenopyrite, stibnite, and various Sb sulfosalts of Pb, Ag and Cu, in a gangue of quartz, baryte and carbonates. At Biò, it is associated with galena, sphalerite, chalcopyrite, pyrite, marcasite, and various Sb sulfosalts of Pb, Ag and Cu, within the same type of gangue. Tubulite is metallic black; optical properties could not be observed under the microscope, due to the crystal morphology. Electron microprobe analysis gave (wt.% - average of 8 anal.): Ag 2.7(2), Pb 46.6(9), Sb 26.1(8), S 17.8(5), Total 93.2(2.1). The low total is due to the thinness of the tube wall. According to crystallographic study (electron and X-ray diffraction), tubulite is monoclinic (space group *Pc*, *P*2/*c* or *P*2_1/*c*) with unit-cell parameters *a* 4.132(2), *b* 43.1(2), *c* 27.4(1) Å, β 93.2°, *V* 4872(40) Å^3, with $Z = 2$. Weak reflections in the [010] electron diffraction pattern indicate a 2*a* superstructure. Main diffraction lines are [d (Å), (*I*)]: 3.99 (*35*), 3.69 (*60*), 3.36 (*100*), 3.28 (*55*), 2.99 (*55*), 2.912 (*55*), 2.063 (*75*). The unit cell of tubulite is very close to those of sterryite and parasterryite; like these sulfosalts, tubulite is probably an expanded derivative of owyheeite. Its peculiar tubular morphology is discussed within the general framework of crystals whose habit presents a circular symmetry. It is proposed that micro-tubes were initiated by capillary forces acting on very thin lamellar crystallites around gas bubbles or liquid droplets.

Key-words: tubulite, new mineral, sulfosalt, lead, silver, tubular morphology, Le Rivet, Peyrebrune, France, Biò, Borgofranco, Italy.

Introduction

In 1998, during the examination, in search of micro-crystals for the preparation of micromounts, of a sampling from Le Rivet quarry (in the area of Peyrebrune Pb–Zn–Ag mine, Tarn department, France), one of us (R. P.) discovered an ore mineral with a very unusual tubular habit, associated with galena and various antimony sulfosalts. Although the mineralogical characterization of this tubular mineral appeared very difficult, due to its peculiar habit, a first scanning electron microscope (SEM) chemical analysis proved it to be a Pb–Ag–Sb sulfosalt with an original composition, distinct from any known mineral species of this group.

In 2002, a new occurrence of what appeared to be the same sulfosalt (first SEM analyses in 2006), with the same tubular habit, was discovered at Biò, in the upper galleries (Veneziana and Torinese) of the Pb–Ag–As–Sb Borgofranco mines (Borgofranco d'Ivrea, Turin, Piedmont, Italy) (*''unknown mineral UKMBB 703''* – Ambrino *et al.,* 2008; Ciriotti *et al.,* 2009 – see cover photo of the latter book). Its study allowed confirming and completing the data obtained on the first, French occurrence. On this basis, it was possible to define this new mineral for which the name 'tubulite' was proposed, due to its original main crystal habit.

The mineral and its name have been accepted by the CNMNC of the IMA, under the number 2011–109.

0935-1221/13/0025-2334 $ 6.30
DOI: 10.1127/0935-1221/2013/0025-2334

Holotype material from Le Rivet quarry is deposited in the collections of the Museum of Mineralogy of the Ecole Nationale Supérieure des Mines de Paris (now MINES ParisTech), France, catalogue number M 82939. Holotype material from Biò is deposited in the mineralogical collections of the Museo Regionale di Scienze Naturali, Via Giovanni Giolitti 36, Turin, Italy, catalogue number 15905. Cotype specimens are deposited in the mineralogical collections of the Museo di Storia Naturale, Università di Pisa, Via Roma 79, Calci, Pisa, Italy, catalogue number 19630, and in the collections of the Musée Cantonal de Géologie, Université-Anthropole, 1015 Lausanne, Switzerland, catalogue number MGL#92635.

Recently, the definition of a new sulfosalt, parasterryite (Moëlo *et al.,* 2011), and the resolution of the crystal structures of parasterryite and sterryite (Moëlo *et al.,* 2012) revealed the close crystal chemical relationship between tubulite and these two sulfosalts, which are expanded derivatives of owyheeite.

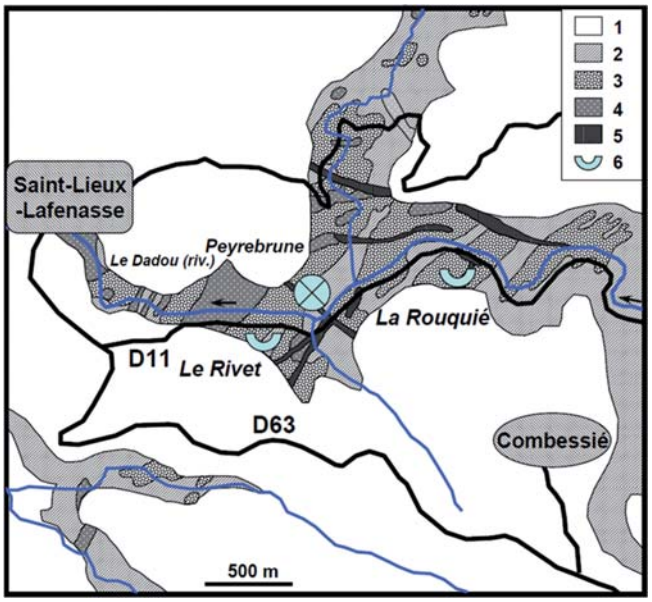

Fig. 2. Geological location of Le Rivet quarry (simplified according to Guérangé-Lozes *et al.*, 1996). 1. Sedimentary cover (Tertiary to Present); 2. Ordovician black schists; 3. Interstratified metadolerites and metabasalts; 4. Hercynian granitic and micro-granitic dykes; 5. Main Pb–Zn mineralized quartz veins of Peyrebrune ore deposit (crossed circle: mine buildings); 6. Quarry.

1. The deposits and their parageneses

1.1. The French deposit of Le Rivet quarry

The quarry of Le Rivet belongs to the Peyrebrune Pb–Zn–Ag ore field, located along the Dadou river, about 6 km E-SE of the town of Réalmont, on the commune of Montredon-Labessonié, Tarn department, France (Figs. 1 and 2). Geographic coordinates of Le Rivet quarry are $x = 43°\ 45'\ 42''$N, $y = 02°\ 14'\ 16''$ E and $z \sim 240$ m. A general review of the nearby Peyrebrune mine (history and exploitation) has been presented by Di Cato (1996). According to Contri (1959), Durand (1966), and Pierrot *et al.* (1976), the ore deposit consists of quartz veins oriented EW; these veins intersect a metamorphosed volcano-sedimentary complex (Ordovician black schists with meta-dolerites and meta-basalts) with some granitic and micro-granitic sills (Peyrebrune granite), indicative of a Hercynian shallow batholith (Durand, 1966; Guérangé-Lozes *et al.,* 1996). This geologic formation occurs at the western margin of Massif Central, in direct contact with the Tertiary cover of the Aquitaine Basin.

The vein system of Peyrebrune was studied in detail by Contri (1959) and Durand (1966). Le Rivet quarry is situated within meta-dolerites and meta-basalts, and is operated for gravel extraction. Three sub-vertical quartz-dolomitic veins (named A to C) were observed in the quarry. Tubulite samples were collected in vein C, oriented NNE-SSW.

The mineral inventory of Peyrebrune ores has been done by Pierrot *et al.* (1976). Main sulfides are galena, sphalerite, pyrite and chalcopyrite, in a gangue of quartz, siderite, fluorite, calcite and dolomite. Various sulfosalts have been

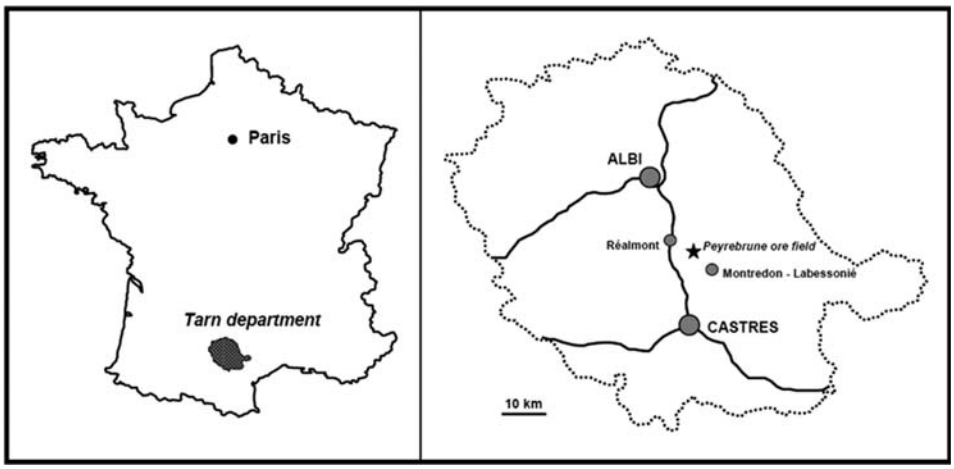

Fig. 1. Geographic location of the Peyrebrune Pb–Zn–Ag ore field. Left: Tarn department in France; right: Peyrebrune in Tarn department.

Table 1. Ore mineral associations at Peyrebrune and Biò.

Peyrebrune	Ref.: Pierrot *et al.* (1976), this study (*: Le Rivet quarry)	
	Gangue	A: quartz*, baryte*, siderite. F: fluorite, calcite*, dolomite*. t: ankerite
	Sulfides	A: galena*. F: pyrite, sphalerite, chalcopyrite. t: marcasite, arsenopyrite, pyrrhotite, stibnite
	Sulfosalts	F: bournonite. t: tetrahedrite-freibergite, semseyite, boulangerite*, freieslebenite, miargyite, polybasite, proustite, pyrargyrite, pyrostilpnite, polybasite, tubulite*, wittichenite
Biò	Ref.: Ambrino *et al.* (2008)	
	Gangue	A: quartz, baryte, calcite, dolomite, siderite
	Sulfides	A: galena, sphalerite. t: orpiment, marcasite, chalcopyrite
	Sulfosalts	F: tetrahedrite-freibergite, bournonite, boulangerite t: semseyite, geocronite, fizélyite, diaphorite, miargyrite, pyrargyrite-proustite, pyrostilpnite, tubulite

A, abundant; F, frequent; t, traces.

observed through the metallographic study, as well as later by mineral collectors (Bernadi, 1992; Hubert & Hubert, 1992) (Table 1).

A detailed sequence of ore deposition has been established by Durand (1966). It can be simplified as follows:

- Stage I: dolomite;
- Stage II (main): galena and sphalerite, in a gangue of siderite;
- Stage III: chalcopyrite with quartz and fluorite;
- Stage IV (discrete): stibnite;
- Stage V: baryte.

Stage II is the main silver carrier. Bournonite is the most abundant sulfosalt, then tetrahedrite. Although they are spatially subordinated to galena and chalcopyrite, it is probable that these minerals and other sulfosalts (among which tubulite) may result for a main part from the remobilization of sulfides of stages II and III by Sb-rich solutions of stage IV (superimposition process).

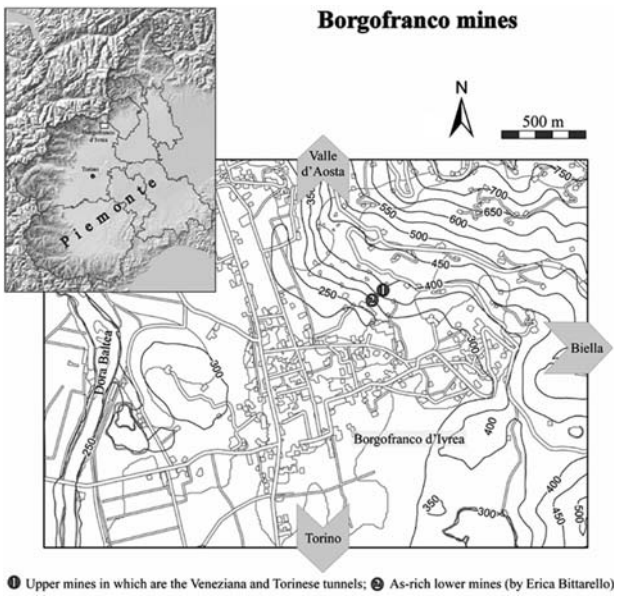

Fig. 3. Location of the Biò occurrences from Borgofranco mine district (reproduced from Ambrino *et al.*, 2008). Veneziana and Torinese tunnels = 1.

1.2. The Italian deposit of Biò, Borgofranco mines

The Borgofranco Pb–Ag–As–Sb ore district is composed of 14 small mines, worked in the past for silver, lead, arsenic and antimony (Lincio, 1916). This ore district is located in Piedmont, around the town of Borgofranco d'Ivrea, situated at about 50 km north of Turin, along the Dora Baltea river, on the road to Val d'Aosta (Fig. 3).

The ore district is located at the foot of Mount Vesino, within the geo-tectonic ''Canavese Zone'' which, according to Baggio & Friz (1969), represents a ''post-Hercynian cover of the Ivrea-Verbano area''. The Canavese Zone is actually composed of fault-bounded tectonic slices which include both pre-Alpine basement and Permo-Mesozoic cover (Borghi *et al.,* 1996); it is a narrow tectonic unit bounded by the western end of the Insubric Line and separating the Sesia Zone (Austroalpine Domain) from the Ivrea Zone (Southalpine Domain) (*e.g.*, Borghi *et al.,* 1996). There, the two domains are separated by the ''tectonic suture'' of the ''Schists of Biò'', known with the name of ''Biò suture''.

Mineralized veins intersect the ''schists of Biò'', a non-fossiliferous sedimentary sequence of mudstones, sandstones, arkoses and impure limestones (Biino & Compagnoni, 1989), probably Upper Jurassic in age (R. Compagnoni, pers. comm. 2012).

The mineralogy of these ores has been detailed by Piccoli *et al.* (2007) and Ambrino *et al.* (2008). The latter authors especially described the sulfosalt association. Main gangue minerals are quartz and baryte, together with carbonates (calcite, dolomite and siderite). Simple sulfides are galena, sphalerite, chalcopyrite, pyrite, marcasite and orpiment; numerous Sb sulfosalts were identified (Table 1).

Tubulite samples have been discovered in 2002 by two of us (B.M. and A.S.) in the two mine tunnels of Veneziana and Torinese, just above the farm of Biò (Fig. 3). Geographic coordinates are $x = 45°\ 31'\ 07''$ N, $y = 7°\ 51'\ 53''$ E, and $z \sim 300$–350 m.

2. Descriptive study

Under the binocular microscope, typical tubulite crystals appear in vugs as rare metallic black cylinders (Fig. 4 a and b), associated with galena, and also boulangerite at Le Rivet. Contrary to natural cylindrite crystals, which are completely filled cylinders (Makovicky, 1971), tubulite crystals, when observed along their elongation axis, appear as perfect tubes with a very thin wall. The SEM images of such a tube (*e.g.*, Fig. 5a) indicate a wall thickness of about 2 μm, for a diameter of several tens of μm, and a length up to 600 μm. The external surface of the tube shows two steps

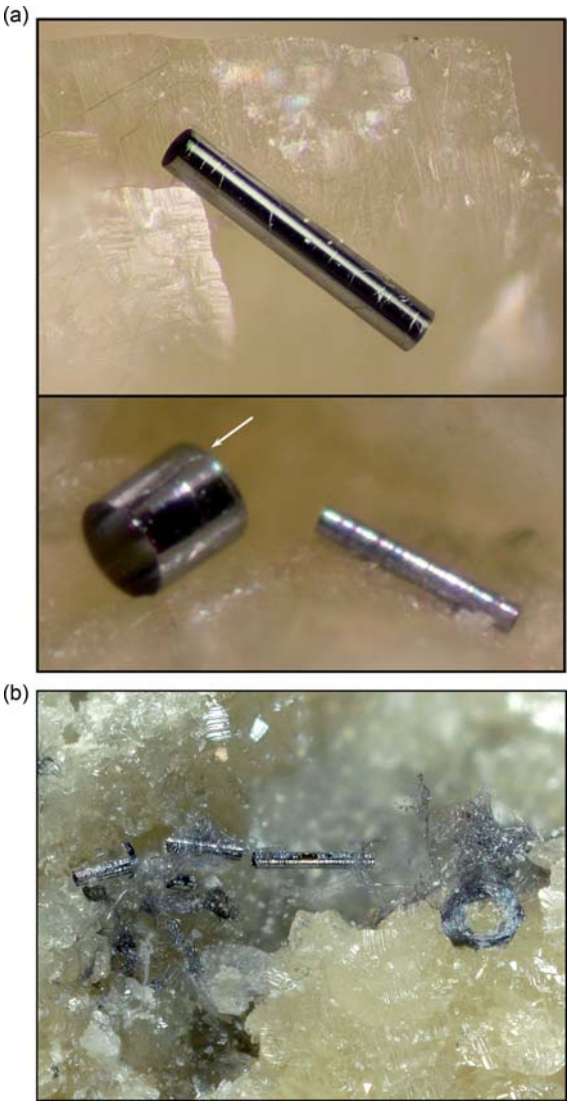

Fig. 4. Photomicrographs of typical tubulite crystals. a) Le Rivet quarry. Top: long tube, 0.4 mm in length (Sample: R. P.; photo courtesy by J.-M. Johannet). Bottom (sample and photo: R. P.): the tube at left (L 0.3 mm, Ø 0.2 mm) shows on its upper part a linear step (parallel to the tube axis - arrow) indicating a spiral growth. Tube at right: L 0.5 mm, Ø 0.05 mm. b) Biò. Several perfect tubes associated with nano-wires of the same sulfosalt (forming a scroll at right) (field size: 2.6 × 3.3 mm; photo by E. Bonacina, reproduced with his authorization).

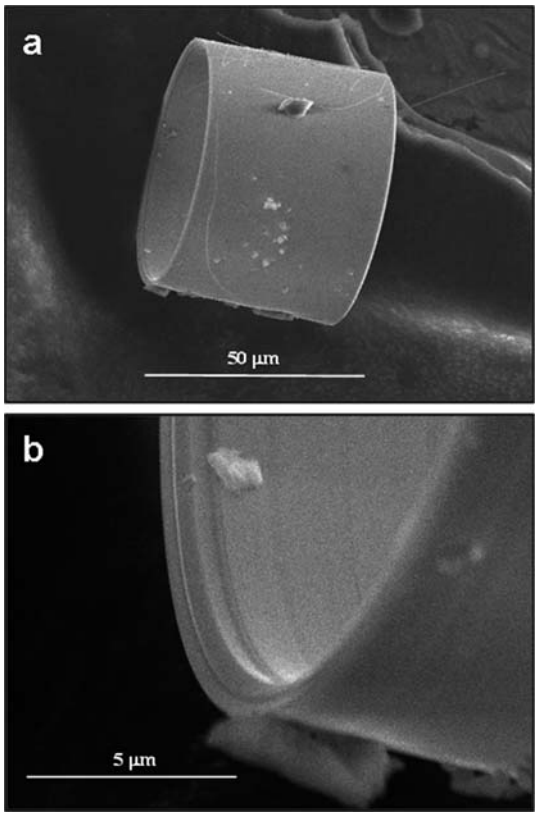

Fig. 5. Scanning electron microscope (SEM) images of a tubulite crystal from Le Rivet quarry: a) general view. Two growth steps (curved lines) are visible on the external surface of the tube; b) detail of one edge.

that would correspond to a spiral growth around the tube axis (also visible in Fig. 4a – tube at left). Rarely were observed unrolled, more or less undulated elongated lamellae, for instance on a crystal face of calcite and baryte at Biò.

Tubulite from Biò (Fig. 4b and 6) is closely associated with geocronite, bournonite, fizélyite, and a hair-like sulfosalt (''*unknown mineral UKMBB708''*of Ambrino *et al.,* 2008), which appeared to be another habit of tubulite (see below). This tubulite variety is constituted by very fine micro-fibres (''nano-wires'' – Fig. 6a), about 0.2 μm thick. Details of a needle-like tip are given in Fig. 6b. When forming a scroll (Fig. 7), with a diameter of about 400 μm, and at least about fifty turns, the length of such a micro-fibre may reach 6 cm, *i.e.* a length/width ratio of $\sim 3 \times 10^5$.

2.1. Physical properties

Optical properties as well as hardness could not be studied, due to the crystal morphology. Tubes show no plasticity, contrary to cylindrite crystals, and appear very resistant to crushing. For instance, one tube sandwiched between two glass lamellae (45 × 30 × 1.5 mm) was not flattened under the lamella weight. Under stronger pressure, the tube broke into rings, then rings into arched fragments. Such fragments were used for TEM study.

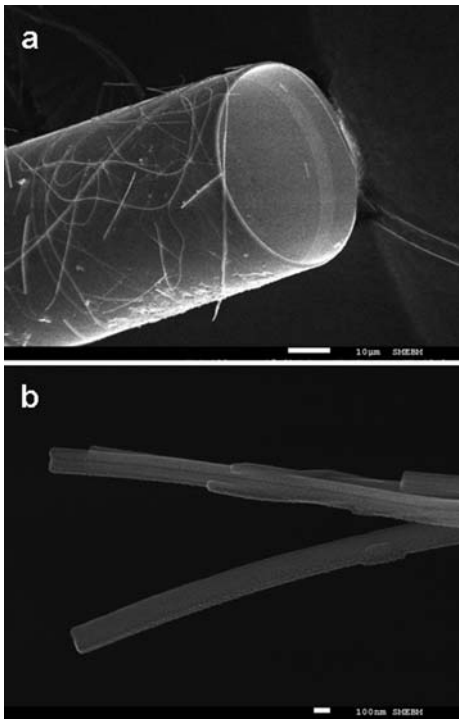

Fig. 6. SEM images of a tubulite crystal from Biò a) General view, the external surface of the tube shows fibres of its hair-like variety (''UKMBB708''); b) tip of a fibre showing several crystals in parallel growth.

Fig. 7. SEM image of a nest-like wire of the fibrous habit of tubulite (Biò).

3. Chemical analysis

Tubulite from Le Rivet was analyzed first, with a SEM equipped with EDS. One tube was put lying on a plot with its cylindrical axis perpendicular to the electron beam, to have the best geometry for quantitative analysis. One tube from Biò was also analyzed later in the same way. Nevertheless, due to the overlapping of S $K\alpha$ and Pb $M\alpha$ peaks with EDS analysis, the peak deconvolution process was not sufficient to obtain an accurate S:Pb:Sb ratio for such a compound. Thus, another tube from Biò was studied by electron probe microanalysis (EPMA) in wavelength-dispersive mode (CAMECA SX 50 apparatus, common laboratory BRGM-CNRS-University of Orléans). Other Pb sulfosalts were also analyzed as secondary standards. The microprobe beam was focused on the top surface of the tube (put horizontally on a flat surface), to prevent any obliquity of its incidence direction.

All these analyses are presented in Table 2. Analytical totals show a more or less significant deficiency, which is due to the thickness of the tube wall, below the excitation volume induced by the electron beam at 20 kV. The SEM analyses revealed only Pb, Sb and S as major chemical components, together with minor Ag. Microprobe analysis confirmed these features and did not reveal any other detectable element ($Z > 10$) in significant amount (above some tenths of wt.%). Figure 8 represents the projection of these analyses in the Pb_2S_2–Sb_2S_3–Ag_2S pseudo-ternary system (equivalent to the Pb–Sb–Ag system), together with the composition of various neighbouring Pb sulfosalts. The SEM analyses of the two occurrences overlap; nevertheless there is a shift between SEM and EPMA analyses of the Biò sample, and the EPMA analysis must be considered as the most accurate reference for tubulite composition. The tubulite compositional field is close to those of members of the owyheeite homologous series: owyheeite (Moëlo *et al.,* 1984a), sterryite and parasterryite (Moëlo *et al.,* 2011), but with a higher Pb content, mainly to the detriment of Ag. Thus, tubulite composition appears as intermediate between that of owyheeite and those of boulangerite and semseyite.

The hair-like variety of tubulite (''UKMBB708'') could be analyzed only with the SEM. Due to the thinness of fibres, chemical analyses show a bad analytical total (from 78 down to 44 wt.%) and a strong dispersion (Fig. 8). The composition of this variety appeared significantly distinct from that of typical tubulite, with a shift toward a higher Pb ratio. Nevertheless, this chemical shift seems to be due to an analytical artefact owing to the small size of the excited volume (in favour of the chemical element with the highest Z), since the X-ray powder diffraction pattern (XRPD) revealed the identity of ''UKMBB708'' with typical tubulite.

4. Crystallographic study

4.1. X-ray diffraction study

4.1.1. Powder diffraction

A preliminary powder X-ray diffraction pattern was obtained on a tube from Le Rivet, using a Gandolfi camera (114.6 mm diameter) and Cu $K\alpha$ radiation (Fig. 9 and Table 3). A tube from Biò gave a similar diagram. Another XRPD pattern obtained on nano-wires of ''UKMBB708'' from Biò appeared identical with that of type tubulite (Fig. 9). Due to the poor quality of the XRPD patterns, and to the high values of b and c parameters, these

Table 2. Electron probe microanalysis of tubulite from Le Rivet quarry and Biò.

	wt.%		Ag	Pb	Sb	S	Total
Le Rivet SEM		1	3.7	40.0	23.4	17.1	84.2
		2	3.5	39.9	23.7	17.0	84.1
Biò							
SEM (EDS)	Mean 12		3.2	41.3	24.1	17.9	86.4
	σ		0.2	1.2	0.9	0.5	1.2
	$\sum = 100$ %		3.7	47.8	27.9	20.7	100.0
	σ		0.2	1.4	1.1	0.5	1.3
EPMA (WDS)	Mean 8		2.7	46.6	26.1	17.8	93.2
	σ		0.2	0.9	0.8	0.5	2.1
	$\sum = 100$ %		2.9	50.0	28.0	19.1	100.0
	σ		0.2	0.9	0.8	0.5	2.2
Unit formula (WDS)			Ag	Pb	Sb	S	Ev (%)
$\sum$ cat. = 5 at.	Mean		0.27	2.42	2.31	5.97	0.8
	σ		0.01	0.03	0.03	0.03	
$\sum$ cat. = 44 at.	Mean		2.4	21.3	20.3	52.5	
	σ		0.1	0.3	0.3	0.3	
$\sum$ cat. = 45 at.	Mean		2.4	21.8	20.8	53.7	
	σ		0.1	0.3	0.3	0.3	

Ev: relative error on the valence balance.

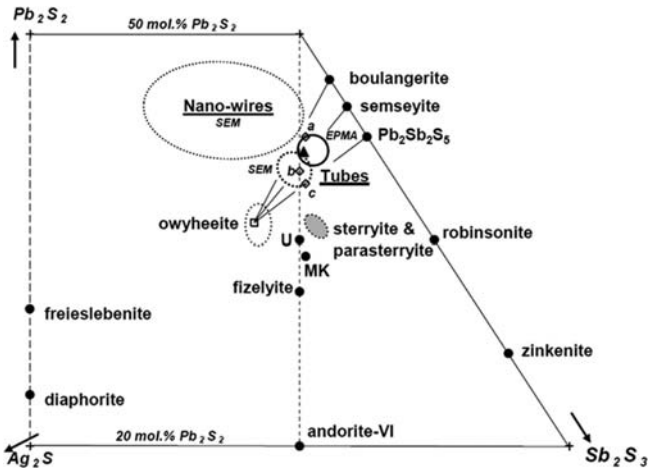

Fig. 8. Projection in the Ag-poor sub-part of the Pb_2S_2–Sb_2S_3–Ag_2S pseudo-ternary system of the analyses of tubulite (tubes and nano-wires). For tubes, the two circles correspond to areas of SEM analyses (Le Rivet and Biò), and EPMA (Biò; black triangle is the mean composition). For nano-wires (Biò), the large ellipse encloses SEM analyses. Solid-solution field of owhyeeite (ellipse) and ideal stoichiometric composition (square – $Ag_3Pb_{10}Sb_{11}S_{28}$) according to Moëlo *et al*., (1984a). Small grey ellipse: compositions of sterryite and parasterryite. U: uchucchacuaite; MK: unknown mineral of Moëlo *et al.* (1989). Lozenges a, b and c: possible ideal compositions of tubulite, $Ag_2Pb_{22}Sb_{20}S_{53}$, $Ag_3Pb_{21}Sb_{21}S_{54}$ and $Ag_3Pb_{20}Sb_{21}S_{53}$, respectively, close to the segments between owyheeite, on the one hand, and, on the other hand, boulangerite, semseyite or synthetic $Pb_2Sb_2S_5$.

patterns could not be indexed to refine the unit cell. Only the strong lines at $d = 3.57$ and 2.063 Å probably correspond to reflections 057 and –201, respectively, according to X-ray single-crystal and TEM studies. In the same figure, comparison with the XRPD patterns obtained for sterryite and parasterryite using the same apparatus (Moëlo *et al.,* 2011) proves the specificity of tubulite diagram.

4.1.2. Single-crystal study

One tubular crystal from Le Rivet was put on a glass capillary using a Nonius Kappa CCD detector. X-ray diffraction data were treated in order to obtain precession images. Figure 10 presents the best image obtained. Two symmetric rectangular nets have been visualized. This symmetry is the result of the cylindrical shape of the single crystal. These patterns correspond to the **b*** × **c*** plane, without any 0*kl* extinction rules.

4.2. TEM study

After crushing, ring fragments of a tube were put on a copper grid coated with holey carbon film, and examined with a Philips CM30 electron microscope operating at 300 kV. Due to the curvature of these fragments, they were lying with their cylinder axis sub-perpendicular to the grid plane (*i.e.* sub-parallel to the electron beam). This permitted to obtain a diffraction pattern (Fig. 11) corresponding to the reciprocal plane perpendicular to the cylinder axis, combining the unit vector **a*** sub-tangential to the tube, and the second vector **c*** parallel to the cylinder radius (radial axis).

Due to the short value of **c*** and the thinness of the tube (**c*** is perpendicular to the tube wall), both the zero- and first-order Laue zones (ZOLZ and FOLZ) overlap, corresponding to *h*0*l* and *h*1*l* reflection sets. The β angle is close to 93.2°. For *h*0*l* reflections, those with odd *l* are absent.

Weak but distinct streaks (arrows on Fig. 11) indicate clearly a disordered 2*a* superstructure (∼ 8 Å), commonly observed in acicular lead sulfosalts.

4.3. Uni-cell parameters

X-ray precession and TEM studies indicate a monoclinic symmetry, with β = 93.2°. According to the [010] electron diffraction pattern, one has:

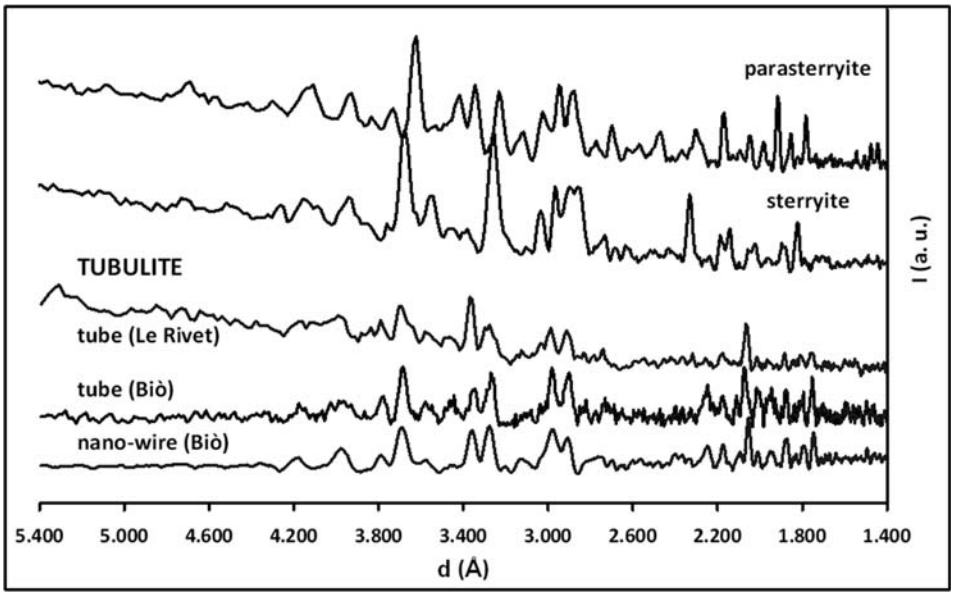

Fig. 9. Tubulite: comparison of X-ray powder patterns of typical tubes (Le Rivet and Biò) and its hair-like variety (Biò), together with those of sterryite and parasterryite. The strong line of tubulite XRPD pattern at ~2.06 Å corresponds to $d_{(-201)}$, that is the layered atom stacking along *a*.

Table 3. Tubulite: X-ray powder diagrams of tubes from Le Rivet quarry and Biò.

Le Rivet		Biò	
d (Å)	*I* relat.	*d* (Å)	*I* relat.
4.18	20		
4.11	30	4.13	20
3.99	**35**		
3.84	15		
3.79	30		
3.69	**60**	3.66	30
3.65	25		
3.57	20*		
3.47	20		
3.36	**100**	3.36	20
3.28	**55**	3.28	20
3.03	25		
2.99	**55**		
2.912	**55**	2.903	20
2.744	25	2.734	10
2.549	10		
2.451	10		
2.421	10		
2.366	10		
2.318	20		
2.257	10		
2.180	20		
2.063	**75****	2.074	100
2.015	15	2.010	10
1.963	15		
1.884	25	1.882	10
1.810	20	1.799	20
1.753	25	1.754	30
1.600	20		

* *hkl* = 057? ** *hkl* = −201?

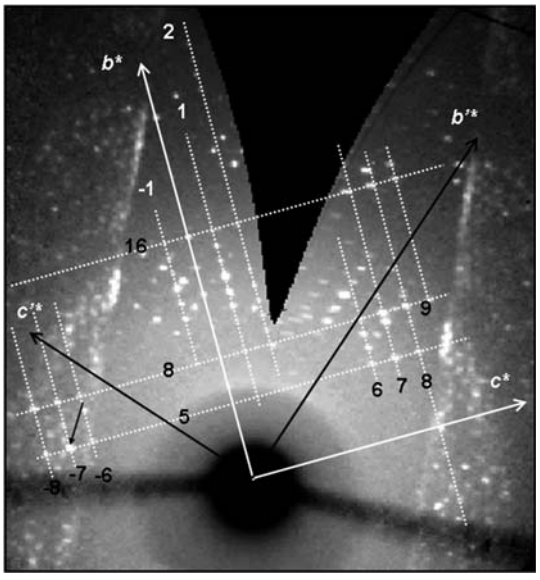

Fig. 10. X-ray precession image on a tubulite crystal from Le Rivet quarry, with crystallographic interpretation according to two symmetric rectangular (**b***, **c***) and (**b'***, **c'***) lattices. Indexation relative to the (**b***, **c***) lattice. Small arrow: strong reflection 05–7 at 3.57 Å ($d_{calc.}$ = 3.559 Å).

– $d_{(100)} \sim 4.12$ Å = $a \sin\beta$, that is $a \sim 4.13$ Å. The strong line of the XRPD pattern at 2.063(1) Å corresponds very probably to the most intense spot of the TEM diffraction pattern, *i.e.*, $d_{(-201)}$, which gives $a = 4.132(2)$ Å.
– and $d_{(001)} \sim 27.38(10)$ Å = $c \sin\beta$, that is $c = 27.42(10) \sim 27.4(1)$ Å.

The X-ray precession image shows the two unit vectors **b*** and **c***. On the basis of the calculated *c* value, one has *b*

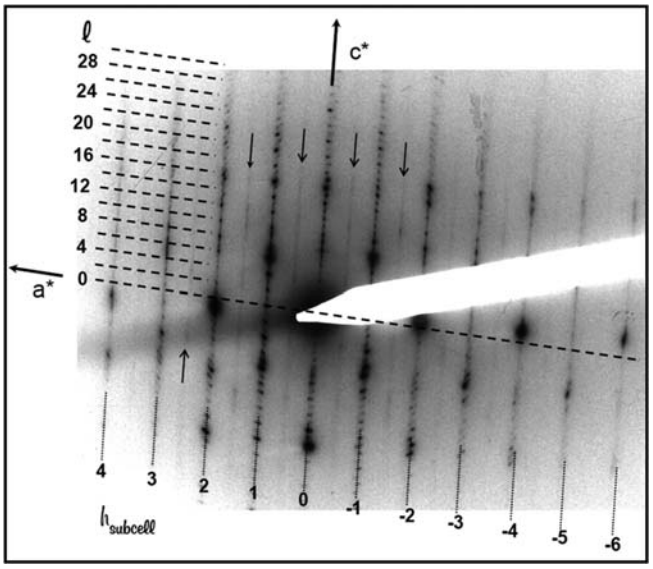

Fig. 11. [010] electron diffraction pattern on a ring fragment from a broken tubulite crystal from Le Rivet quarry. Small arrows: diffuse streaks corresponding to a disordered 8 Å superstructure.

$\sim$ 43.1(2) Å. The **b** axis, perpendicular to **a** and **c**, is parallel to the tube axis. Figure 12 represents the orientation of the unit-cell vectors relatively to the tube wall.

With these unit-cell parameters (Table 4), the unit-cell volume is $V = 4872(40)$ Å^3, that of the $\sim$8 Å superstructure is 9758 Å^3.

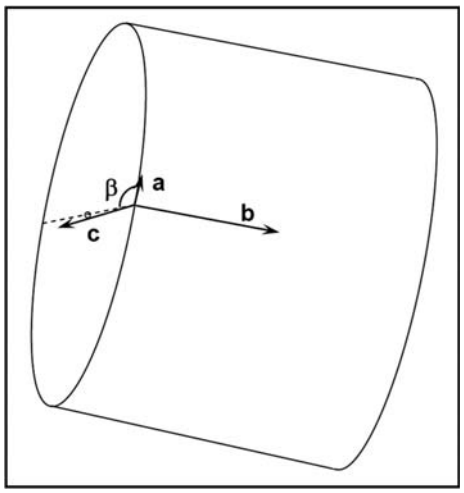

Fig. 12. Orientation of unit-cell parameters relatively to the tubular morphology.

As the electron diffraction pattern indicates the reflection condition $h + l = 2n$, while the X-ray precession image indicates no extinction conditions for $0kl$ indices, possible space groups are $P2/c$ (No. 13), or the non-isomorphic subgroups $P2_1/c$ (No. 14) or Pc (No. 7).

5. Relationship with other lead sulfosalts and unit-cell content

5.1. Similarities with sterryite and parasterryite

Crystal size and tubular morphology preclude any crystal structure refinement of tubulite by X-ray diffraction. The very small thinness of its hair-like variety at Biò puts obstacles as well to a structure study. Nevertheless, some characteristics of the unit cell, together with the chemical formula, permit to envisage a structural relationship with some other sub-groups of Pb sulfosalts.

First, the shortest parameter, close to 4 Å ($\times$ 2), evidently relates to a structure derived from the PbS or SnS archetypes, like most lead sulfosalts (Makovicky, 1985a; 1993). Its high value (4.13 Å) points to three possible series of Pb sulfosalts: 1) zinkenite series (Makovicky, 1985b), 2) andorite-lillianite series or 3) sartorite series (Makovicky, 1997). Although the chemical composition of tubulite quite agrees with the general formula of the andorite series, $Ag_xPb_{3-2x}Sb_{2+x}S_6$ ($x \sim 0.30$), as indicated by Table 2 and Fig. 7, and its Pb/Sb atomic ratio (1.46 $\sim$ 3/2, after subtracting Ag), this series admits only high values of x, and the lowest value ($x = 0.5$) corresponds to uchucchacuaite, $AgMnPb_3Sb_5S_{12}$ (Moëlo *et al.,* 1984b; Moëlo *et al.,* 1989), and its As-rich derivative menchettiite, $AgMn_{1.6}Pb_{2.4}Sb_3As_2S_{12}$ (Bindi *et al.,* 2012), which are stable only with Mn partly substituting Pb. Moreover, all members of this series of homeotypes have three similar (sub-)parameters in common ($\sim$4.3, 13 and 19 Å), which is not the case for tubulite.

Members of the sartorite homologous series have two close (sub-)parameters, $\sim$8.0 and 4.2 Å (Makovicky, 1985a). The $\sim$8 Å parameter does not fit with any of those of tubulite, and all these compounds contain major As, without pure Sb members.

On the contrary, as indicated by Table 4, the unit cell of tubulite is very similar to those of sterryite and parasterryite, the two closest Pb–Ag–Sb sulfosalts (Fig. 7). Its supercell volume (9758 Å^3) is significantly below those of sterryite and parasterryite. As these two sulfosalts

Table 4. Comparison of unit cells of tubulite and members of the owhyeeite group.

	a (Å)	*b* (Å)	*c* (Å)	β (°)	Space group	*V* (Å^3)
Owyheeite [1]	4.1035	27.3144	22.9366	90.359	$P2_1/c$	2571
Sterryite Madoc [2]	28.4	42.6	8.26	90	*Pba*2 or *Pbam*	9921
Sterryite Pollone [3]	8.1891	28.5294	42.98	94.896	$P2_1/n$	10005
Parasterryite [3]	8.3965	27.954	43.884	90.061	$P2_1/c$	10300
Tubulite [4]	4.132(2) (x2)	43.1(2)	27.4(1)	93.2	$P2/c$, Pc or $P2_1/c$	4872(40) (x 2)

[1] Laufek *et al*. (2007); [2] Jambor (1967); [3] Moëlo *et al.* (2011); [4] this study.

contain a significant amount of As substituting Sb, their hypothetical Sb-pure derivatives would have a higher unit-cell volume. Thus tubulite cannot be such a Sb-pure derivative, and its unit-cell atom content must be lower than those of sterryite and parasterryite. This is also confirmed by the specificity of the XRPD pattern of tubulite (Fig. 8).

Sterryite and parasterryite belong to the same space group $P2_1/c$ (No. 14), that would favour the same choice for tubulite among the three possible ones. But, contrary to sterryite and parasterryite, where the β angle is between the shortest (∼8.2–8.4 Å) and the longest parameters (∼43–44 Å), that of tubulite is between the shortest and the intermediate (∼27 Å) parameters. All three possible space groups for tubulite imply $Z = 1$, 2, or also $Z = 4$ for No. 13 and 14.

5.2. Structural formula

The unit-cell content of tubulite can be approximated by comparison with the unit-cell contents of sterryite and parasterryite. One knows that the volume V_{ex} of a complex ''molecule'', here the unit formula of a complex sulfosalt, is close to the addition of the volumes V_{Sulf} of the unit formulas for the simple sulfides that constitute this ''molecule'', according to their ratios in the structural formula (Moëlo, 1983). For instance, let us consider semseyite, $Pb_9Sb_8S_{21}$, whose unit formula corresponds to the sum of 9 PbS plus 4 Sb_2S_3 (Table 5):

- the unit-cell volume of PbS (galena) is 208.95 Å^3, with $Z = 4$; thus the volume V_{PbS} of a single ''molecule'' PbS is 52.24 Å^3;
- the unit cell volume of Sb_2S_3 (stibnite) is 487.72 Å^3, with $Z = 4$; thus the volume V_{Sb2S3} of one Sb_2S_3 is 121.93 Å^3.
- therefore one has $9\ V_{PbS} + 4\ V_{Sb2S3} = 957.88$ Å$^3 = V_{mix}$, the calculated volume of the mixture of galena and stibnite with the semseyite formula,
- while the effective unit-cell volume of semseyite is 3816.49 Å^3, with $Z = 4$. The exact volume V_{ex} of $Pb_9Sb_8S_{21}$ is 954.12 Å^3.

Thus one has $V_{mix}/V_{ex} = 1.0039$: the relative error is only +0.39 %, which shows the accuracy of this approximation. The same holds for boulangerite, $Pb_5Sb_4S_{11}$, for which $V_{mix}/V_{ex} = 0.9998$. Table 5 also applies this approach to owyheeite (Moëlo *et al.,* 1984a; Laufek *et al.,* 2007), as well as to sterryite and parasterryite from Pollone (Italy - Moëlo *et al.,* 2011), for which $V_{mix}/V_{ex} = 0.994$, 1.008 and 1.009, respectively. For tubulite, on the basis of the microprobe analysis (and proposed $Z = 2$, as in sterryite and parasterryite), the two unit formulas with an integer number of cations that approximate the ideal value of V_{ex} correspond to 44 and 45 cations ($V_{mix}/V_{ex} = 0.993$ and 1.017, respectively). To 44 cations correspond 52.95 S atoms (ideally 53), to 45 cations, 54.15 S atoms (ideally 54). The two

Table 5. Calculated unit-formula volumes (V_{mix}) of tubulite and close Pb–Sb–(Ag) sulfosalts, compared to their experimental volumes (V_{ex}).

Simple sulfides		PbS	Sb_2S_3	As_2S_3	AsS	Ag_2S	Cu_2S	V_{mix}	V_{ex}	V_{mix}/V_{ex}
Molar volume (Å^3)		52.24	121.93	117.12	49.97	56.80	45.65			
Sulfosalts	Unit formula									
Semseyite	$Pb_9Sb_8S_{21}$	x 9 = 470.2	x 4 = 487.7					957.9	954.1	1.004
Boulangerite	$Pb_5Sb_4S_{11}$	x 5 = 261.2	x 2 = 243.9					505.1	505.2	0.9998
Owyheeite	$Ag_3Pb_{10}Sb_{11}S_{28}$	x 10 = 522.4	x 11/2 = 670.6			x 3/2 = 85.2		1278.2	1285.5	0.994
Sterryite	$Cu(Ag,Cu)_3Pb_{19}$-$(Sb,As)_{22}(As{-}As)S_{56}$	x 19 = 992.6	x 8 = 975.4	x 3 = 351.4	x 2 = 100.0	x 1 = 56.8	x 1 = 45.7	2521.9	2501.3	1.008
Parasterryite	Ag_4Pb_{20}-$(Sb_{14.5}As_{9.5})_{\sum 24}S_{58}$	x 20 = 1044.8	x 14.5/2 = 884.0	x 9.5/2 = 556.3		x 2 = 113.6		2598.7	2575.0	1.009
Tubulite	$Ag_{2.4}Pb_{21.8}Sb_{20.8}S_{53.7}$	x 21.8 = 1140.4	x 20.8/2 = 1266.6		x 1.2 = 70.7			2477.7	2436(20)	1.017
	$Ag_{2.4}Pb_{21.3}Sb_{20.3}S_{52.5}$	x 21.3 = 1112.7	x 20.3/2 = 1237.5		x 1.2 = 68.2			2418.4	2436(20)	0.993

For each sulfosalt: first line = number of simple-sulfide molecules in its unit formula; second line = calculated partial volume. For tubulite, two formulas are considered.

formula units calculated with 44 and 45 cations on the basis of the microprobe analysis are $Ag_{2.4}Pb_{21.3}Sb_{20.3}S_{52.5}$ and $Ag_{2.4}Pb_{21.8}Sb_{20.8}S_{53.7}$, respectively (Table 2). According to the substitution rule Ag + Sb ↔ 2 Pb, the first formula is intermediate between the stoichiometries $Ag_2Pb_{22}Sb_{20}S_{53}$ (1) and $Ag_3Pb_{20}Sb_{21}S_{53}$ (2). The only stoichiometric formula close to the second one is $Ag_3Pb_{21}Sb_{21}S_{54}$ (3). These three ideal formulas have been indicated in the triangular diagram of Fig. 7. Without the knowledge of the crystal structure, the formula (1), *i.e.* $Ag_2Pb_{22}Sb_{20}S_{53}$, the closest to the microprobe analysis, will be considered as the ideal formula of tubulite for the time being.

On the basis of this unit formula, $Ag_2Pb_{22}Sb_{20}S_{53}$, and $Z = 2$, the calculated density of tubulite is $D = 6.06(5)$ g/cm^3, between those of owyheeite, semseyite and boulangerite (6.03, 6.15 and 6.20 g/cm^3, respectively).

5.3. What structural type for tubulite?

The crystal chemical peculiarities of tubulite point to a crystal structure probably derived by expansion from that of owyheeite, as demonstrated for sterryite and parasterryite (Moëlo *et al.,* 2011, 2012). It would signify an organization around complex rods with pseudo-triangular symmetry, constituting the basic building block of owyheeite (Laufek *et al.,* 2007). It has also been indicated that the crystal structure of parasterryite can be interpreted as a unit-cell intergrowth of two types of building blocks, one of the owyheeite type, the second of the sartorite type, their chemical mixture giving the chemical composition of parasterryite.

Similarly, it is possible to view tubulite as a chemical mixture between owyheeite and a Pb–Sb sulfosalt (see Fig. 7), *i.e.* boulangerite for formula (1), semseyite for formula (3), or synthetic $Pb_2Sb_2S_5$ (Skowron & Brown, 1990) for formula (2). It is thus probable that the tubulite structure contains building sub-units of one among these three Pb–Sb sulfosalts.

6. Tubular morphology and genesis of crystal habits with circular symmetry: discussion

6.1. Crystal habits with circular symmetry

The formation of the same new compound in two distinct deposits with such an original tubular morphology cannot be explained for the time being, especially because its crystal structure is unknown. For comparison and discussion, one can review schematically the different types of crystal habits presenting strong regular curvature, *i.e.* circular symmetry. A first inventory of such habits in the field of mineralogy was done by Bideaux (1970). These habits are rings, disks, massive cylinders, tubes, helix and spheres.

- Rings are well known in the group of acicular Pb–Sb sulfosalts, particularly jamesonite and boulangerite (Bideaux, 1970; Mielke, 1977; Ghiurca, 1985; Stalder *et al.,* 1998). In Apuan Alps, boulangerite scrolls have been observed in the Seravezza marble (Orlandi *et al.,* 1996), and in the Monte Rocca stope, Bottino mine (Biagioni, 2009). Other scrolls of acicular lead sulfosalts have been observed in the cavities of the Carrara and Massa marble quarries, and in the fractures of the dolostones of the Monte Arsiccio mine (C. Biagioni, writ. com.). A ring of a synthetic Pb–Sb sulfosalt was obtained by Heuer *et al*. (2004). Axial flat rings (*i.*e. short sections of a tube) give circular ribbons, or strips (in synthetic $NbSe_3$–Tsuneta *et al.,* 2003), and constitute an intermediate with thin tubes, while radial flat rings evolve towards disks.
- The most famous example of massive cylindrical crystals is that of cylindrite, described since the end of the XIXth century at Poopo, Bolivia (Frenzel, 1893; Makovicky, 1971). This mineral belongs to the group of composite structures of the 2D misfit type (Makovicky & Hyde, 1992). Numerous synthetic compounds of the same family have also been obtained, sometimes with a tubular habit (Guemas *et al.,* 1988). The oxy–sulfide tochilinite, of the misfit type, also forms cylinders (Zolensky & Mackinnon, 1986). Among pure oxide compounds, chrysotile is well known to form cylindrical growth with polygonal organisation (Baronnet & Devouard, 2005).
- A spiral string of boulangerite (?) in fluorite from Madoc (Canada) was presented by Bideaux (1970). At Wannenköpfe (Eifel massif, Germany), fibrous hematite was also observed with such a morphology (Valverde, 2002).
- Radial growth of curved lamellas gives spherules with onion structure. Such a habit is well known for muscovite in pegmatites, and has also been observed in hisingerite, a ferric derivative of kaolin (Eggleton & Tilley, 1998).
- Other minerals sometimes present a tubular morphology at the micrometric or nanometric scale, for instance chrysotile (Maser *et al.,* 1960; Yada, 1971; Veblen & Buseck, 1979), hollandite (Belkin & Libelo, 1987), halloysite (Bates *et al.,* 1950; Kogure *et al.,* 2011), and tochilinite (Zolensky & Mackinnon, 1986). Such tubes have been also described in boulangerite (at Madoc – Bideaux, 1970), and in synthetic chalcogenides of the 2D-misfit type, *i.e.* ~ $PbNb_2S_5$ (Guemas *et al.,* 1988), as well as ~ $BiNbS_3$ or ~ $BiNb_2S_5$ (Gómez-Herrero *et al.,* 2000).
- Various curved micro- and nanostructures of graphite derivatives have been observed in nature (Jaszczak *et al.,* 2007, and references therein).

Table 6 summarizes these different crystal habits with circular symmetry.

6.2. Genesis of crystals with circular symmetry: discussion

Bideaux (1970) has reviewed the various possible mechanisms generating curved crystals. In many cases, surface

Table 6. Simplified classification of single crystals with habit presenting a circular symmetry.

Crystal anisotropy	A/B/C ratios	Circular symmetry	Curvature axis	Crystal habit
Fibre	A >> B >> C	1D	⊥ A	Scroll, ring
		1D + Translation // circular axis	⊥ A	Spiral
Ribbon	A > B >> C	1D	// B	Flat ring
		1D	// C	Disk
		1D + Translation // circular axis	// B or C	Ribbon spiral
Lamella	A ∼ B >> C	1D	⊥ A	Tube
		2D	// *A* + // B	Hollow sphere
	A ∼ B > C	1D	⊥ A	Cylinder
		2D	// *A* + // B	Full sphere

A, B, C: Three orthogonal vectors, with decreasing size, defining the intrinsic anisotropy of the crystal morphology (before deformation by the circular symmetry).

curvature appears clearly as the consequence of an asymmetric interface at the crystal structure level (curvature of *intrinsic origin*). For instance, in halloysite structure, the connection within the constitutive layer between a SiO_4 tetrahedral sub-layer and an AlO_4 octahedral sub-layer induces a tubular curvature, the ideal (regular) periodicity of the octahedral sub-layer being smaller than that of the tetrahedral sub-layer (Bates *et al.,* 1950). As the layer stacking is obtained through weak hydrogen bonds, if crystal nucleation permits to generate a nanotube, its continuous crystal growth up to a higher, micro- or macroscopic level to form a cylinder is possible due to the flexibility of the layer interface through such hydrogen bonds.

More generally, nanotubes are governed by intrinsic parameters at the unit-cell level (crystallographic mismatch; energetic constraints), as indicated by Krivovichev (2008). In non-commensurate sulfides of the 2D-misfit type, structures consist of the regular alternation of two types of layers (pseudotetragonal Q, and pseudohexagonal H), with an asymmetric interface (like a unit-cell syntactic intergrowth), as exemplified by the crystal structures of cylindrite (Makovicky *et al.,* 2008) and its Cu derivative, lévyclaudite (Evain *et al.,* 2006). In natural Bolivian cylindrite, the tangent of the cylinders is parallel to the **b** parameter pair with b_Q/b_H = 5.790/3.670 Å (Makovicky, 1976). The non-commensurate Q/H interface is permitted owing to the plasticity of the coordination of Pb atoms ($N = 6$ or 7) of the Q layer with the S atoms of the H layer (of the CdI_2 type). The strongest constraint in the interface bonding is the interlayer charge transfer, as 2 Sb^{3+} substituting 2 Pb^{2+} in the Q layer are coupled to 1 Fe^{2+} substituting 1 Sn^{4+} in the H layer, forming rows parallel to the cylinder axis (Makovicky, 1974 – see his Fig. 10). A last important characteristic is the small long-range misfit along the **b** direction, as 4.5 $b_Q = 26.055$ Å ∼ 7 $b_H = 25.690$ Å, *i.e.* a relative difference of only 1.4 % (against ∼2 % between tetrahedral and octahedral sub-layers of serpentine). In synthetic Sn–Se cylindrite (Makovicky *et al.,* 2008), this difference is smaller: 4.5 $b_Q = 26.861$ Å ∼ 7 $b_H = 26.816$ Å, and $\delta_b = 0.2$ %.

According to these crystal-chemical characteristics, the nucleation of a cylindrite crystal, starting from a single pair of the two constitutive H and Q layers, may induce a curvature along **b** of intrinsic origin, like in serpentine, to form a nanotube, whose growth will permit the formation of a cylinder at the macroscopic scale. In layered sulfides, another possible mechanism of formation of a tube or cylinder may result from the syntactic nucleation of two close species, with very close intra-layer parameters. For instance, cylindrical intergrowths of homologues within the family of Pb/Nb/S 2D misfits, together with pure NbS_2, have been described by Moëlo *et al*. (1995). Comparison of intralayer parameters of the NbS_2 H layer (ortho-hexagonal sub-cell) of two homologues (Wiegers & Meerschaut, 1992) with those of NbS_2 (rhombohedral polytype) gives: NbS_2 (orthohexagonal choice): *a* 3.330, *b* 5.768 Å; $(PbS)_{1.14}NbS_2$: *a* 3.313, *b* 5.801 Å; $(PbS)_{1.14}(NbS_2)_2$: *a* 3.326, *b* 5.775 Å. The relative difference δ between *a* or *b* values is always below 1 %.

On the other side, contrary to these cases where the asymmetry of the crystal structure appears to be a prerequisite for the formation of cylindrical morphology, the direct formation, at the macroscopic scale, of tubes or rings would have an *extrinsic origin*. For instance, in the example of ribbon rings observed by Tsuneta *et al*. (2003), the curvature of an $NbSe_3$ synthetic crystal is the consequence of its growth at the surface of a selenium droplet. This example confirms the possible role of spherical droplets in a crystallization medium hypothesized initially by J. Arem (cited by Bideaux, 1970) for the formation of single crystals with circular morphology. Similarly, boulangerite rings at Madoc (Ontario) have been interpreted as the consequence of growth by capillarity around oil droplets (Mielke, 1977).

For jamesonite and boulangerite, which do not have a layered structure, and do not belong to any homologous series, an intrinsic origin of rings is unlikely, all the more because the ring diameter is variable even in a given sample, and the hypothesis of extrinsic formation at a two-liquid interface (water/oil) proposed at Madoc by Mielke (1977) appears very attractive. For tubulite, as tubes are observed in carbonate cavities, one may also consider such a hypothesis; another similar alternative could be the formation of bubbles of carbonic gas through weak dissolution of these carbonates by acid solutions

during sulfosalt deposition. Like selenium or oil droplets, such bubbles may have attracted by capillarity very thin lamellar crystallites of tubulite, inducing a circular growth. The variable diameter of the tubes would thus correspond to a change in the bubble radius.

Crystallites of tubulite with a needle-like morphology may have grown also around a droplet or bubble, but such morphology induces a higher degree of freedom (curvature) during the growth, giving the final scroll observed under the binocular microscope (Fig. 4b), and not perfect rings.

The difference between typical tubular and hair-like morphologies of tubulite is the consequence of distinct ratios of growth speeds along unit-cell vectors (v_a, v_b and v_c). Tubular crystals are derived from ribbon-like crystallites, with $v_a > v_b >> v_c$. Due to mechanical constraints and capillarity strengths, the ribbon would have grown flat along the equatorial circle of an oil droplet or gas bubble, to give a tube through spiral rolling-up. In hair-like crystals, one has $v_a >> v_b \sim v_c$. Such a difference in morphology may be the consequence of twinning, as, according to Grigoriev (1965), a twin contact acts like a defect and favours the growth of twinned crystals along their common twin boundary. In tubulite, (001) as a twin plane, giving a pseudo-orthorhombic symmetry, would favour the growth along **a** and **b** [(001) as twin contact] relatively to **c**, and thus the initiation of ribbon-like crystallite. Twinning would be a structural pre-requisite for the formation of tubular crystals, relatively to untwinned fibrous crystals.

A very similar morphological duality between tubes and fibres was described by Belkin & Libelo (1987). Here it corresponds to crystals of cryptomelane-hollandite growing within Permian bedded salt. According to these authors, the cylinders ''always occur in or very near fluid inclusions''. Individual fibres are commonly ''curved when in a fluid inclusion''. It is important to cite the mechanism invoked by these authors: ''Only one cylinder per fluid inclusion is found in the chevron salt whereas multiple cylinders are commonly found in inclusions in clear salt. The common multiple cylinders in the clear salt may reflect a concentration process that occurred during dissolution and recrystallization of the primary chevron salt. Cylinders trapped in chevron salt would perhaps remain as a residue after salt dissolution and might be trapped in the less common but much larger fluid inclusions characteristic of the clear salt (...) Two important features that are observed are (1) these salt-hosted cylinders are usually near larger inclusions ($> 10\ \mu m^3$) and (2) they occur above the inclusion, in the stratigraphic sense, suggesting that the inclusions may have moved downward, leaving the cylinders behind''.

It is curious that Belkin & Libelo (1987) exclude the role of gas bubbles, when their description strongly suggests such a mechanism: only one bubble within each primary fluid inclusion will permit only one tubular crystal to grow, at the top of this inclusion, while later the coalescence of inclusions through salt recrystallization will permit to observe several tubes within one inclusion.

7. Conclusion

Tubulite appears as a new sulfosalt species of the pseudo-ternary Ag_2S–PbS–Sb_2S_3 system, with the lowest Ag content within the group of Ag–Pb–Sb sulfosalts. Its unit cell is close to those of sterryite and parasterryite, the nearest compounds in the $(Ag,Cu)_2S$–PbS–$(Sb,As)_2S_3$ system. In sulfosalt systematics (Moëlo *et al.,* 2008), this crystal-chemical relationship relates tubulite with the owyheeite sub-group in the zinkenite family. Its crystal structure may correspond to the unit-cell intergrowth of two building blocks, an owyheeite-type complex column and another one derived from a Pb–Sb sulfosalt. A high-resolution transmission electron microscopy (HRTEM) study of fragments of tubular crystals would appear as the best approach in the future to confirm such a structural organization, as exemplified by Kryukova *et al*. (2005) for the structural characterization of the synthetic iodine derivative of pillaite, belonging also to the zinkenite family. On the other hand, one may hope to find flat crystals of sufficient size for an X-ray single-crystal structure study.

The perfect tubular morphology of typical tubulite crystals seems to be related to extrinsic conditions of formation (capillary forces) acting on very thin lath-like crystallites at the beginning of crystal growth. The hypothesis of growth around gas bubbles, or oil droplets, in hydrothermal solutions would need fluid inclusion studies in the two deposits to be confirmed. Tubulite may be also present in other deposits; for instance, sulfosalt tubes (stacked rings) were described by Woodside *et al*. (2000) in the hydrothermal Pb–Zn–Ag–Sb vein system of Van Silver mine (Brandywine Creek, British Columbia, Canada). The SEM analysis of one tube (Y.M.) indicated owyheeite, but the close association in this ore of various Pb–Ag–Cu–Sb sulfosalts, among which boulangerite, semseyite, owyheeite and also fizélyite (Yang *et al.,* 2009), whose compositions surround that of tubulite, may have also favoured the formation of tubulite here. Tubular boulangerite from Madoc observed by Bideaux (1970) with SEM, but apparently without precise chemical analysis, may also correspond to tubulite, close (but without arsenic) to the pair boulangerite-sterryite, present at Madoc (Jambor, 1968; Jambor *et al.,* 1982).

Acknowledgements: We sincerely thank Georges Favreau (Association Française de Microminéralogie - AFM), who actively promoted the study of the French occurrence of tubulite, then the Franco-Italian collaboration, and Giovanni Dalla Fontana for his contribution to the find of the first specimens of tubulite from Biò. The kind help of Cristian Biagioni (Pisa University) and Matteo Boscardin (Museo di Archeologia e Scienze Naturali G. Zannato of Montecchio Maggiore), who provided the preliminary analysis of Italian samples, was also greatly appreciated. Michel Evain (Institut des Matériaux J. Rouxel) helped us in the X-ray precession study. Jean-Marc Johannet (AFM) provided a beautiful photograph of tubulite. Many thanks to Silvio Maccagno who provided the first samples

from Biò studied in Lausanne in 2007, and to Erica Bittarello (Dipartimento di Scienze della Terra – Turin University) for the map of the Italian deposit. We finally thank Professor E. Makovicky (University of Copenhagen) and Dr. A. J. Locock (University of Alberta) for their constructive comments, as well as S. Krivovichev, Chief Editor of the *European Journal of Mineralogy*, for his careful monitoring of the manuscript.

References

Ambrino, P., Blass, G., Boscardin, M., Ciriotti, M.E., Dalla Fontana, G., Kolitsch, U., Martini, B., Milli, L., Salvetti, A., Bonacina, E. (2008): Borgofranco d'Ivrea. La paragenesi a solfuri e solfosali delle miniere argentifere. *Riv. Mineral. Ital.*, **3/2008**, 144–162.

Baggio, P. & Friz, C. (1969): Fenomeni tettonico-metamorfici di età alpina lungo la linea Insubrica auct. *Mem. Mus. Trid. Sci. Nat.*, **17**, 183–206.

Baronnet, A. & Devouard, B. (2005): Microstructures of common polygonal serpentines from axial HRTEM imaging, electron diffraction, and lattice-simulation data. *Can. Mineral.*, **43**, 513–542.

Bates, T.F., Hildebrand, F.A., Swineford, A. (1950): Morphology and structure of endellite and halloysite. *Am. Mineral.*, **35**, 463–484.

Belkin, H.E. & Libelo, E.L. (1987): Fibers and cylinders of cryptomelane-hollandite in Permian bedded salt, Palo Duro Basin, Texas. *Am. Mineral.*, **72**, 1211–1224.

Bernadi, G. (1992): Peyrebrune: Carrière du Rivet. *Cahier Des Micromonteurs*, **1**, 3–10.

Biagioni, C. (2009): Minerali della Provincia di Lucca. Associazione Micro-mineralogica Italiana éd., Cremona, 352 p.

Bideaux, R.A. (1970): Mineral rings and cylinders. *Mineral. Rec.*, **1**, 105–112.

Biino, G. & Compagnoni, R. (1989): The Canavese Zone between the Serra d'Ivrea and the Dora Baltea river (Western Alps). *Eclog. Geol. Helvet.*, **82** (2), 413–427.

Bindi, L., Keutsch, F.N., Bonazzi, P. (2012): Menchettiite, $AgPb_{2.40}Mn_{1.60}Sb_3As_2S_{12}$, a new sulfosalt belonging to the lillianite series from the Uchucchacua polymetallic deposit, Lima Department, Peru. *Am. Mineral.*, **97**, 440–446.

Borghi, A., Compagnoni, R., Naldi, M. (1996): The crystalline basement of the Canavese Zone (Internal Western Alps): new data from the area west of Ivrea (Northern Italy). *Géologie Alpine*, **72**, 23–34.

Ciriotti, M.E., Fascio, L., Pasero, M. (2009): Italian type minerals. Plus-Pisa university press ed., Pisa, 357 p.

Contri, J.P. (1959): Etude géologique et métallogénique des environs de Peyrebrune et de Montroc près Réalmont (Tarn). Thesis, Paris University, 127 p.

Di Cato, P. (1996): Peyrebrune: Une mine dans le Tarn. Graphitarn éd., Albi, 190 p.

Durand, B. (1966): Le gisement plombo-zincifère de Peyrebrune, Tarn (France). Thesis, Nancy University, 251 p.

Eggleton, R.A. & Tilley, D.B. (1998): Hisingerite: A ferric kaolin mineral with curved morphology. *Clays Clay Minerals*, **46**, 400–413.

Evain, M., Petricek, V., Moëlo, Y., Maurel, C. (2006): First (3 + 2)-dimensional superspace approach to the structure of levyclaudite-(Sb), a member of the cylindrite-type minerals. *Acta Cryst. B*, **62**, 775–789.

Frenzel, A. (1893): Über den Kylindrit. *N. Jb. Miner. Geol. Paläont.*, **2**, 125–128.

Ghiurca, V. (1985): Les habitus en rondelles. Dans le monde curieux des microcristaux de jamesonite. *Minér. & Fos.*, **120**, 22–30.

Gómez-Herrero, A., Landa-Cásanovas, A.R., Hansen, S., Otero-Díaz, L.C. (2000): Electron microscopy study of tubular crystals $(BiS)_{1+d}(NbS_2)_n$. *Micron.*, **31**, 587–595.

Grigoriev, D.P. (1965): Ontogeny of minerals. Israel Program for Scientific Translation éd., Jerusalem, 250 p.

Guemas, L., Rabu, P., Meerschaut, A., Rouxel, J. (1988): Characterization of new ''$SnNbS_3$, $PbNbS_3$, $PbNb_2S_5$, $SnTiS_3$ and $SnTi_2S_5$'' compounds. *Mater. Res. Bull.*, **23**, 1061–1069.

Guérangé-Lozes, J., Mouline, M.P., Delsahut, B. (1996): Geological map of France (1/50000): Réalmont (959). BRGM éd., Orléans.

Heuer, M., Wagner, G., Döring, T., Bente, K., Kryukova, G. (2004): Nanowire arrangements of $PbS–Sb_2S_3$ compounds. *J. Crystal Growth.*, **267**, 745–750.

Hubert, M.-N. & Hubert, M. (1992): A propos du gisement de Peyrebrune: Histoire d'une de nos découvertes. *Cahier Des Micromonteurs*, **2**, 27–33.

Jambor, J.L. (1967): New lead sulfoantimonides from Madoc, Ontario. Part 2 – Mineral descriptions. *Can. Mineral.*, **9**, 191–213.

— (1968): New lead sulfoantimonides from Madoc, Ontario. Part 3 – Syntheses, paragenesis, origin. *Can. Mineral.*, **9**, 505–521.

Jambor, J.L., Laflamme, J.H.G., Walker, D.A. (1982): A re-examination of the Madoc sulfosalts. *Mineral. Rec.*., **13**, 93–100.

Jaszczak, J.A., Dimovski, S., Hackney, S.A., Robinson, G.W., Bosio, P., Gogotsi, Y. (2007): Micro- and nanoscale graphite cones and tubes from Hackman valley, Kola Peninsula, Russia. *Can. Mineral.*, **45**, 379–389.

Kogure, T., Mori, K., Kimura, Y., Takai, Y. (2011): Unraveling the stacking structure in tubular halloysite using a new TEM with computer-assisted minimal-dose system. *Am. Mineral.*, **96**, 1776–1780.

Krivovichev, S.V. (2008) Nanotubes in minerals and mineral-related systems. *in*''Minerals as advanced materials I'', S. Krivovichev, ed., Springer, Berlin/Heidelberg, 179–191.

Kryukova, G.N., Heuer, M., Wagner, G., Doering, T., Bente, K. (2005): Synthetic $Cu_{0.507}Pb_{8.73}Sb_{8.15}I_{1.6}S_{20.0}$ nanowires. *J. Solid State Chem.*, **178**, 376–381.

Laufek, F., Pažout, R., Makovicky, E. (2007): Crystal structure of owyheeite, $Ag_{1.5}Pb_{4.43}Sb_{6.07}S_{14}$: refinement from powder synchrotron X-ray diffraction. *Eur. J. Mineral.*, **19**, 557–566.

Lincio, G. (1916): Note preliminari su alcuni minerali del giacimento metallifero di Borgofranco d'Ivrea. *Rend. R. Accad. Naz. Lincei.*, **25**, 227–230.

Makovicky, E. (1971): Microstructure of cylindrite. *N. Jb. Mineral. Mh.*, **1971**, 403–413.

— (1976): Crystallography of cylindrite. *N. Jb. Mineral. Abh.*, **126**, 304–306.

— (1985a): The building principles and classification of sulfosalts based on the SnS archetype. *Fortschr. Miner.*, **63**, 45–89.

— (1985b): Cyclically twinned sulphosalt structures and their approximate analogues. *Z. Kristallogr.*, **173**, 1–23.

— (1993): Rod-based sulphosalt structures derived from the SnS and PbS archetypes. *Eur. J. Mineral.*, **5**, 545–591.

— (1997): Modular crystal chemistry of sulphosalts and other complex sulfides. *in* ''Modular aspects of Minerals''. *EMU Notes in Mineralogy*, **1**, 237–271.

Makovicky, E. (1974): Mineralogical data on cylindrite and incaite. *N. Jb. Miner. Mh.*, **1974**, 235–256.

Makovicky, E. & Hyde, B.G. (1992): Incommensurate, two-layer structures with complex crystal chemistry: minerals and related synthetics. *Mat. Sci. Forum*, **100 & 101**, 1–100.

Makovicky, E., Petříček, V., Dušek, M., Topa, D. (2008): Crystal structure of a synthetic tin-selenium representative of the cylindrite structure type. *Am. Mineral.*, **93**, 1797–1798.

Maser, M., Rice, R.V., Klug, H.P. (1960): Chrysotile morphology. *Am. Mineral.*, **45**, 680–688.

Mielke, R. (1977): Boulangerite and associated minerals of the Rogers mine, Madoc, Ontario. Unpub. B. Sc. thesis, University of Waterloo, Waterloo, Ontario.

Moëlo, Y. (1983): Contribution à l'étude des conditions naturelles de formation des sulfures complexes d'antimoine et plomb. Thesis, Series *Documents du BRGM*, **57**, BRGM ed. (Orléans), 624 p.

Moëlo, Y., Mozgova, N., Picot, P., Bortnikov, N., Vrublevskaya, Z. (1984a): Cristallochimie de l'owyheeite: nouvelles données. *Tschermaks Min. Petr. Mitt*., **32**, 271–284.

Moëlo, Y., Oudin, E., Picot, P., Caye, R. (1984b): L'uchucchacuaite, $AgMnPb_3Sb_5S_{12}$, une nouvelle espèce minérale de la série de l'andorite. *Bull. Minéral*., **107**, 597–604.

Moëlo, Y., Makovicky, E., Karup-Møller, S. (1989): Sulfures complexes plombo-argentifères: minéralogie et cristallochimie de la série andorite-fizélyite. Series *Documents du BRGM*, **167**. BRGM éd. (Orléans), 107 p.

Moëlo, Y., Meerschaut, A., Rouxel, J., Auriel, C. (1995): Precise analytical characterization of incommensurate sandwiched layered compounds $[(Pb,Sn)S]_{1+x}[(Nb,Ti)S_2]_m$ ($0.08 \leq \leq 0.28$, $m = 1$–3). Role of cationic coupling on the properties and the structural modulation. *Chem. Mater*., **7**, 1759–1771.

Moëlo, Y., Makovicky, E., Mozgova, N.N., Jambor, J.L., Cook, N., Pring, A., Paar, W.H., Nickel, E.H., Graeser, S., Karup-Møller, S., Balic-Zunic, T., Mumme, W.G., Vurro, F., Topa, D., Bindi, L., Bente, K., Shimizu, M. (2008): Sulfosalt systematics: a review. Report of the sulfosalt sub-committee of the IMA Commission on Ore Mineralogy. *Eur. J. Mineral*., **20**, 7–46.

Moëlo, Y., Orlandi, P., Guillot-Deudon, C., Biagioni, C., Paar, W., Evain, M. (2011): Lead-antimony sulfosalts from Tuscany (Italy). XI. The new mineral parasterryite, $Ag_4Pb_{20}(Sb_{14.5}As_{9.5})_{\sum=24}S_{58}$, and associated sterryite, $Cu(Ag,Cu)_3Pb_{19}(Sb_{18-15}As_{4-7})_{\sum=22}(As–As)S_{56}$, from Pollone mine (Tuscany, Italy). *Can. Mineral*., **49**, 623–638.

Moëlo, Y., Guillot-Deudon, C., Evain, M., Orlandi, P., Biagioni, C. (2012): Comparative modular analysis of two complex sulfosalt structures: sterryite, $\sim Cu(Ag,Cu)_3Pb_{19}(Sb,As)_{22}(As–As)S_{56}$, and parasterryite, $Ag_4Pb_{20}(Sb,As)_{24}S_{58}$. *Acta Cryst. B*, **68** (5), 480–492.

Orlandi, P., Del Chiaro, L., Pagano, R. (1996): Minerals of the Seravezza Marble, Tuscany, Italy. *Mineral. Rec*., **27** (1), 47–58.

Piccoli, G.C., Maletto, G., Bosio, P., Lombardo, B. (2007): Minerali del Piemonte e della Valle d'Aosta. Associazione Amici del Museo ''F. Eusebio'' Alba ed., Alba (Cuneo), 607 p.

Pierrot, R., Picot, P., Fortuné, J.-P., Tollon, F. (1976): Inventaire minéralogique de la France No 6: Tarn (81). Service Géologique National (BRGM) ed., Orléans, 147 p.

Skowron, A. & Brown, I.D. (1990): Structure of $Pb_2Sb_2S_5$. *Acta Cryst. C*, **46**, 534–536.

Stalder, H.A., Wagner, A., Graeser, S., Stuker, P., Offerman, E., Meisser, N. (1998): Mineralienlexikon der Schweiz. Wepf & Co. ed., Basel, 579 p.

Tsuneta, T., Tanda, S., Inagaki, K., Okajima, Y., Yamaya, K. (2003): New crystal topologies and the charge-density-wave in $NbSe_3$. *Physica B*, 329–333, 1544–1545.

Valverde, J. (2002): Photo p. 32. *Cahier des Micromonteurs*, **78**–**4**.

Veblen, D.R. & Buseck, P.R. (1979): Serpentine minerals: Intergrowths and new combination structures. *Science*, **206**, 1398–1400.

Wiegers, G.A. & Meerschaut, A. (1992): Misfit layer compounds $(MS)_nTS_2$ (M = Sn, Pb, Bi, Rare Earth metals; T = Nb, Ta, Ti, V, Cr; $1.08<n<1.23$): Structures and physical properties. *Mater. Sci. Forum*, **100 & 101**, 101–172.

Woodside, R.W.M., Soregaroli, A.E., Ansell, H.G., Twaites, B.L., Balacko, T.W. (2000): Rare sulfosalts from the Van Silver Mine, British Columbia. *Mineral. Rec*., **31** (3), 219–229.

Yada, K. (1971): Study of microstructure of chrysotile asbestos by high resolution electron microscopy. *Acta Cryst. A*, **27**, 659–664.

Yang, H., Downs, R.T., Burt, J.B., Costin, G. (2009): Structure refinement of an untwinned single crystal of Ag-excess fizélyite, $Ag_{5.94}Pb_{13.74}Sb_{20.84}S_{48}$. *Can. Mineral*., **47**, 1257–1264.

Zolensky, M.E. & Mackinnon, I.D.R. (1986): Microstructures of cylindrical tochilinites. *Am. Mineral*., **71**, 1201–1209.

Received 23 May 2013
Modified version received 1 July 2013
Accepted 22 July 2013